Local Structuring of Diketopyrrolopyrrole (DPP)-based Semiconducting Polymers using Molecular Dynamics Simulations

Maryam Reisjalali, J.Javiér Burgos-Marmól, and Alessandro Troisi

Department of Chemistry, University of Liverpool, Crown Place, Liverpool, L69 7ZD

E-mail: m.reisjalali@liverpool.ac.uk

Abstract

High performing organic semiconducting polymers show great potentials for use in electronic devices which is greatly dependent on the material crystallinity and packing. A series of short oligomers of the diketopyrrolopyrrole (DPP)-based materials that have shown to have high charge mobility are studied to understand the local structuring at atomic level for these materials. The simulations show that the tendency for this material class to form aggregates is driven by the interaction between DPP fragments, but this is modulated by the other conjugated fragments of the materials which affect the rigidity of the polymer and the ability to form aggregates of larger size.

Introduction

The use of organic semiconducting polymers (SCP) in electronic devices has been a great topic of interest in research and material development for many years due to their environmental stability, easy solution processability, flexibility[1,2] and most importantly, their exhibited high charge carrier mobility. These materials have applications across fields such

as the active layer of field-effect transistors (FETs),[3,4] organic photovoltaics (OPVs)[5,6] and bioelectronics[7–9] with reported mobilities as high as $\sim$ 10 cm^2 V^{-1} s^{-1}.[10,11]

Despite many years of investigation, the relation between polymer structure and charge transport property remain unclear. Following the analogy with inorganic semiconductors in which polycrystalline materials are more favoured to enhance charge transport, semicrystalline organic semiconductors such as P3HT (poly(3-hexylthiophene)) , PQT (poly(3,3-dialkyl-quaterthiophene)) and PBBTTT were extensively studied for a long while.[12] Do et al.[13] calculated higher hole mobility in the polymer PBTTT than P3HT for TFTs due to a higher order of planarity, closer and more parallel stacking of the chains that facilitate inter and intra-molecular charge transport and theoretical works started focusing on the crystalline phase.[14,15] Despite the high volume of research on the more crystalline SCPs such as P3ATs, a study by Noriega et al. in 2012 changed the dynamic of the field by stating that long-range ordering is not essential for high charge carrier mobility and only short-range stacking is efficient as long as there exist long chains connecting ordered domains. Experimental support has also been provided for this statement by showing the existence of ordered domains for a range of polymers varying from semicrystalline P3HT to intermediates such as PDPPBT and amorphous such as Rr-P3HT and DPP-based polymers using grazing incidence x-ray diffraction (GIXRD) experiments.[16] However, the effect of other structural properties such as aggregation, local ordered domains and segregation of different parts of the polymeric chains on the performance of such materials have not been studied extensively[17,18] which is greatly due to the complex nature of these materials. The numerous possible ways of making a semiconducting polymer, from selection of the segment along the conjugated backbone, different chain lengths, different alkyl side chain length or having a planar or branched side chain results in many studies in the field, yet the lack of a generalised understanding of the behaviour of these materials.

The backbone of a polymeric chain mainly consists of a selection of aromatic rings and a choice of alkyl side chains to provide solubility in solutions and adjusting the aggregation.[4,19] The degree of crystallinity in this class of materials was shown to be influenced by changing the ratio of branched additives and the side chains used.[20] Some of these varieties are the size and length of the side chain,[21,22] whether a branched-chain enhances the device performance compared to a planar chain, the length and planarity of the backbone, as well as the type of conjugating aromatic rings. Interdigitation of side chains observed by XRD for polythiophenes has been shown to be an important factor for the formation of crystallites for PBTTT[17] which does not affect for the case of P3HT.[23] Jackson et al.[24] have computationally studied a group of polymers that all have high charge carrier mobilities, however, found that they undergo a wide range of different conformational ordering as a result of the change in their chemical structure. Tamaya et al.[25] showed in their article that increasing the number of thiophene rings in the backbone of a DPP polymer chain results in reducing bandgap as well as a shift of the absorption to higher wavelengths. Yiu et al. investigates the effect of changing thiophene rings in the backbone of a polymeric system with a furan ring (PDPP2FT and PDPP3T) as well as the effects of having branched or planar alkyl chains. Increasing the planarity of the chain by replacing thiophene rings by Furan[26,27] has been observed by GIXRD to result in better stacking and aggregation. Lee et al.[28] investigated the effect of having different conjugated segments in the backbone by changing between thiophene rings to the infused thienothiophenes as well as changing the length of the alkyl side chain from 2-hexyldecyl (HD) or 2-octyldodecyl (OD). Based on experimental techniques of synchrotron X-ray diffraction and atomic force microscopy (AFM), they showed that the more planar backbones and longer side chains result in more crystalline structure. Changing the length of the side chains in a polymeric system causes an asymmetry in the density of the charge donating and accepting parts modulating the degree of crystallinity for those systems. Existence of more conjugated units along the backbone, on the other hand, remains a larger space for the interdigitation of side chains, therefore, enabling the formation of larger

crystalline regions. The effect of the number of carbon atoms before the branching position in a branched side chain has been shown to increase the interchain π-π stacking by Meager et al.[29] Ashraf et al.[30] shows that using a bigger heteroatom in a polymeric system, such as replacing sulphur with selenium, results in a stronger intermolecular interaction, therefore, a higher degree of π-stacking. XRD showed peaks of up to fourth-order for PDPPTT-Se. Tang et al.[31] observe the appearance of different aggregate conformations (H and J-aggregates) in the absorption spectra of thiazole containing DPP thin-film transistors with the change of alkyl side chain length. Zhang et al.[32] study the effect of the polymeric chain end groups by choosing pyrene instead of conventional hydrogen atoms or thiophene rings as end groups. They have shown that due to the effect of the pyrene-pyrene interactions and the imposed self-assembly on the planarity of the chains, there is an enhancement in the ambipolar properties of the devices realised as well as the effect of the end groups with respect to the number of DPP moiety in the backbone.

SCPs belonging to DPP-based family are promising materials for use in electronic devices due to their reported high charge carrier mobility.[28,33–35] They can be classified as a paracrystalline material meaning they undergo short-range ordered domains while do not form an overall crystalline structures.[36] The DPP units strong electron-withdrawing nature when combined with appropriate electron donating moeities, make a good candidate for an ambipolar device to be used in organic solar cells, FETs and OLEDs.[37–40] TFT devices realised using ambipolar DPP-based materials were one of the first devices to report NIR light emission.[11] Having different conjugation segments between the DPP units have a direct effect on the planarity of the chains, therefore, enhancing the charge carrier mobility.[41] Fused aromatic rings such as TT have a high tendency to form π-π stacking resulting in high mobility.[42,43] Remarkable aggregation properties are observed for this class of material using different experimental techniques such as grazing incidence X-Ray diffraction (GIXRD), XRD, atomic force microscopy (AFM) and tunneling electron microscopy (TEM).[25,30,33,44]

Classical simulations have contributed to the understanding of semiconducting polymers since the emergence of the field.[5,45–51] Mollinger et al.[52] in their study propose a theoretical approach to understand the underlying physics of charge transport in a material with ordered regions in an overall paracrystalline material. State of the art molecular dynamic (MD) simulations can be used to further further investigate characteristics of polymer chains at different length scales.[47] Henry et al.[53] use MD and simulated GIXRD to predict the morphological characteristics of benzodithiophene-thienopyrrolodione (BDT-TPD) and further validate its accuracy by comparing with experimental results. However, one can also notice that, due to the complications of performing MD simulations on SCPs such as optimisation of the force-field (FF), large system size and limitations of the time scales feasible for a simulation, the theoretical aspect of this field of research is unable to keep up with the evergrowing number of polymers experimentally realised.

In the following, we develop a relatively fast approach techniques enabling us to study as many polymeric systems with different variations to better understand the underlying reason for their special properties. Three different combinations of SCPs belonging to the DPP-based family of polymers are chosen with reported high charge carrier mobilities.[54–58] Studying a family of related compounds may help discriminating between the general feature of polymers containing the DPP fragment and aspect that are more sensitive to the overall chemistry of the polymer. The alkyl side chains for all the systems are kept the same and as a branched alkyl chain at position 2. Branched side chains in position 2 have been shown to represent the best solubility in solutions. Different combinations of moieties are used in the backbone ranging from 2 thienothiophenes (2TT) rings, 4 thiophene rings (4T) and 6 thiophene rings (6T) to study the effect of their difference and similarities in the overall morphology of the polymeric systems. Molecular dynamics (MD)[59] simulation techniques are used to investigate the existence of local ordering in these three polymers to understand

the underlying reason for their reported high charge mobility.

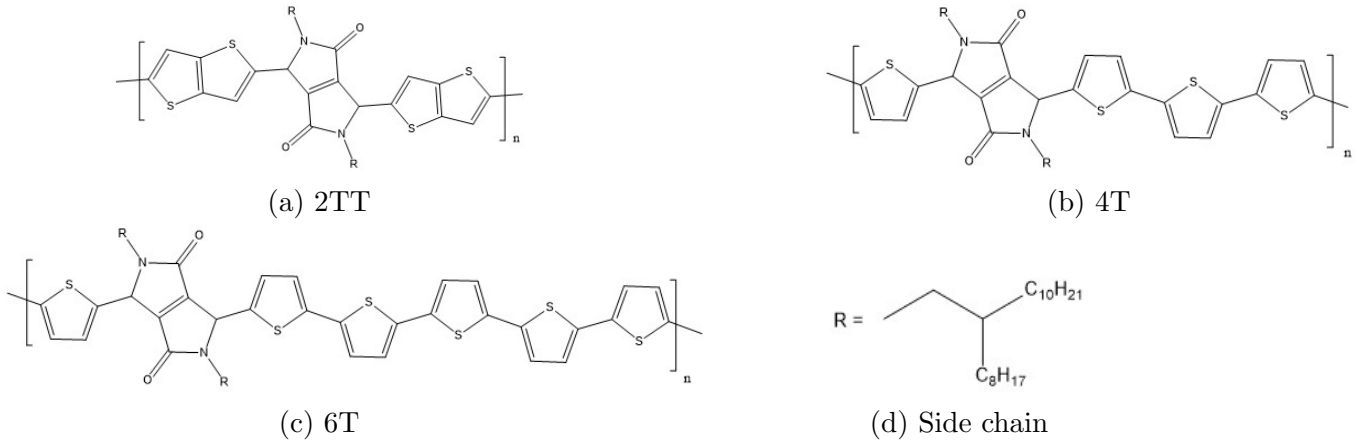

(a) 2TT (b) 4T

(c) 6T (d) Side chain

Figure 1: Chemical structure of the three systems used in this study.

Methods

Force-Field

The molecular model employed in the present work is based on an implementation of All-atom Optimised Potentials for Liquid Simulations[60] (OPLS) force-field to describe the energetic terms of bonded and non-bonded potentials. The force-filed employed in this work includes four harmonically bonded terms (bond stretching, bond angle bending and torsional) and two non-bonded terms (van der Waals (vdW) and Coulomb). The atomic point charges were computed on a trimer of each of the systems optimised using DFT method at B3LYP/6-311G** level via charges from electrostatic potentials using a grid-based method (CHelpG).[61] A chain of three repeating units was used for optimisation, however, the point charges on the atoms of the backbone of the middle monomer were extracted and used for all the repeat units. Point charges of the side chain atoms were taken directly from OPLS-AA force-field. Charge-neutrality of the oligomer chain was obtained by distributing the remaining charges evenly between the sulphur atoms of the system. To calculate the torsional potential in the system, all the rings in the backbone were kept planar. All the parameters for the torsional

potential between alkyl side chain atoms were taken from OPLS-AA. The torsional potential between the rings were calculated using an interpolation table of every 10 degrees dihedral potential calculated using single point MP2[62,63] calculations. The full force field is available within the supporting information.

Simulation Details

In this work, simulations are performed on systems consisting chains of three repeat units of the systems mentioned previously. All the MD simulations are performed using Large-scale Atomic/Molecular Massively Parallel Simulator (LAMMPS).[64] Velocity verlet algorithm was adopted and periodic boundary conditions were applied in all directions with a time step of 2 fs while rattle algorithm is used to constrain H-X bonds. Nóse-Hoover isothermal barostat and thermostat were used to control the ensemble properties. Particle-particle particle-mesh electrostatic summation was used during production simulations with the cutoff of 12 $\mathring{A}$.

The oligomers studied here form glassy phases at room temperature that are difficult to equilibrate (and to verify they are equilibrated). The primary focus of this paper is to study the aggregation property of DPP polymers in equilibrated and highly reproducible phases above the glass transition temperature (Tg). To establish the simulation temperature, simulated annealings are performed on all three systems from 1000 K to 100 K at a rate of 0.02 K/ps. This process was repeated three times to make sure that annealings were performed for long enough and a plausible rate. The three sets were all performed at the same rate where the last point of one run is taken to start the next run by instantly heating it up to 1000 K and slowing cooling to 100 K at the given rate. Annealing processes have been shown to improve structural ordering in the films as evidenced by X-ray scattering and atomic force microscopy.[23,65] Figure.2 represents the inverse density as a function of temperature for the three systems during three sets of simulated annealings. The glass transition temperature (T_g) is found to be similar and around 520 K for the three systems with no significant differ-

ence between the three sets of simulations. The production runs were, therefore, performed at a temperature above T_g. Production simulations were performed from the last point of the second set of simulated annealings for the three systems in an NPT ensemble at 550 K for 400 ns with integration timestep of 2 fs.

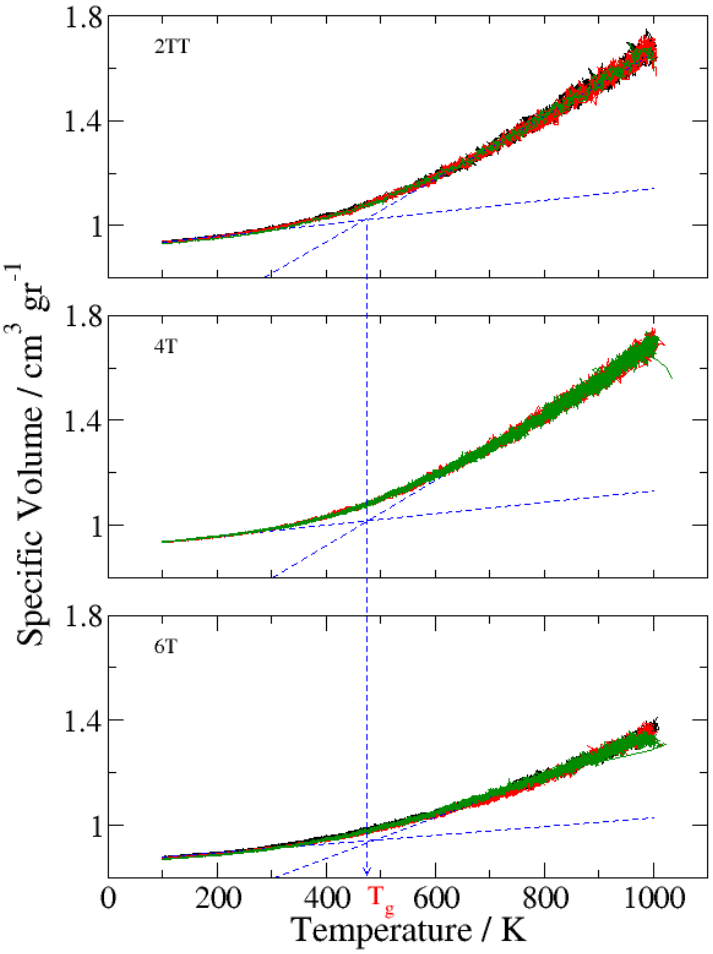

Figure 2: Graphs presenting the inverse of density as a function of the simulated annealing temperature. The glass transition temperature is found by the intersection point between the two linear fits of the graphs. It is shown that the three sets of simulated annealings result in no significant difference in the curves. The glass transition temperature is around the same point (520 K) for all three systems.

Results and Discussions

Production simulations are performed on systems of 64 chains of three repeat units for each of the systems. However, 2TT underwent a box elongation resulting in a much smaller simulation box in the x-direction compared to the other two. Another set of simulation was, therefore, performed on 2TT in which the simulation box in doubled in x-direction resulting in having double the number of chains in this system called 2TTx2 here onwards. Simulations specifications are provided in Table.1.

Table 1: Simulation specification for the production simulations.

Polymer	Atoms /trimer chain	Number of chains	Number of atoms/ simulation
2TT	458	64	29312
2TTx2	458	128	58624
4T	482	64	30848
6T	524	64	33536

Figure.3 represent a snapshot of the simulation boxes for the systems suggesting the presence of local ordering in this class of materials. More analytical and further investigation of topological characteristics such as differences in flexibility of chains as well as for different parts of the chains and local orderings are performed below.

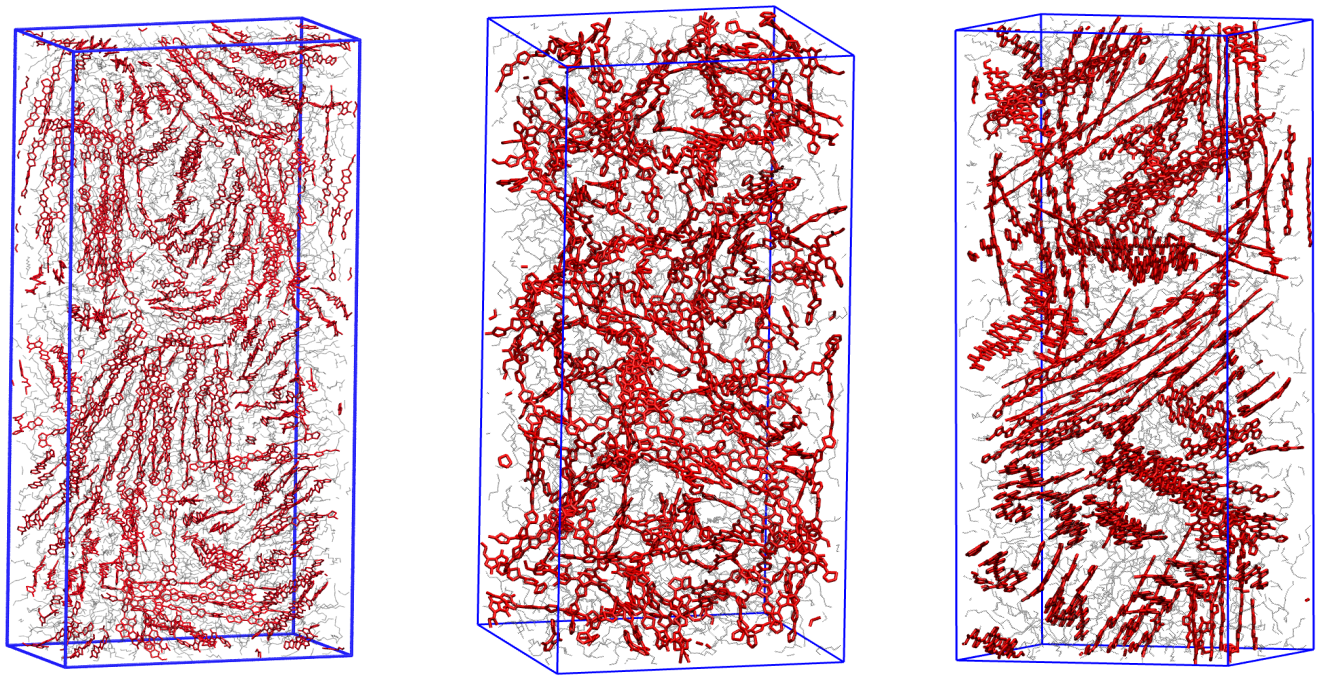

(a) 2TT (b) 4T (c) 6T

Figure 3: Presentation of simulation boxes of the three polymers. The backbones are shown in red and the chain atoms in grey while hydrogen atoms are omitted for simplicity. 2TT and 6T appear to show more rigid chains that result in more visible π-stacking.

Radius of gyration (R_g) and End-to-End distance (D_{ee})

A structural property to determine the flexibility of the polymeric chains and to study their conformation is the radius of gyration (R_g) defined as:

$$R_g = \sqrt{\frac{1}{M}\sum_{i=1}^{n}(\vec{R_i} - \vec{R_{cm}})^2} \tag{1}$$

where M is the total mass of a chain, R_{cm} is the centre of mass position and R_i is the position of each atom in the chain of n atoms. R_g is computed for individual chains as well as an ensemble average for the 64 chains. Another property of the polymeric chains calculated to determine the rigidity of the chains is the end-to-end distance (D_{ee}). End-to-end distances are computed as the distance between the two closing hydrogen atoms at either end of a chain. Comparing this value to that of an isolated fully elongated chain at 0 K indicates

of how coiled the chains are. Table.2 shows comparative values of D_{ee} at 550 K and 0 K and R_g for the three systems. Comparative representation of the most coiled and the most elongated chains are presented in Figure.4 for each system. The figures show that the three polymers are exhibiting different ranges of flexibility. The largest standard deviation of R_g for 4T indicates that has more flexible individual chains followed by 2TT and the least coiled of 6T. A large difference between the values of average D_{ee} and min D_{ee} for 4T shows that individual chains of 4T undergo a wider range of flexibility compared to the other two systems, however, still maintain the overall rigidity.

Table 2: Calculated ensemble average of radius of gyration and its standard deviation during 400 ns production run at 550 K. R_g^0 for a single chain at 0 K is used as an indication of how coiled the chains are.

System	$\bar{R}_g/\mathring{A}$	Standard Deviation $/\mathring{A}$	Minimum R_g $/\mathring{A}$	R_g^0 $/\mathring{A}$
2TT	15.25	0.02	13.55	15.74
2TTx2	15.24	0.02	13.55	15.74
4T	16.38	0.13	10.41	15.91
6T	19.52	0.03	17.99	19.55

Table 3: Calculated ensemble average of end-to-end distance and its standard deviation during 400 ns production run at 550 K. D_{ee}^0 for a single chain at 0 K is used as an indication of how coiled the chains are.

System	$\bar{D}_{ee}/\mathring{A}$	Standard Deviation $/\mathring{A}$	Minimum D_{ee} $/\mathring{A}$	D_{ee}^0 $/\mathring{A}$
2TT	12.25	0.02	11.09	12.77
2TTx2	12.45	0.02	11.09	12.77
4T	12.20	0.40	0.74	12.86
6T	16.81	0.03	14.93	17.03

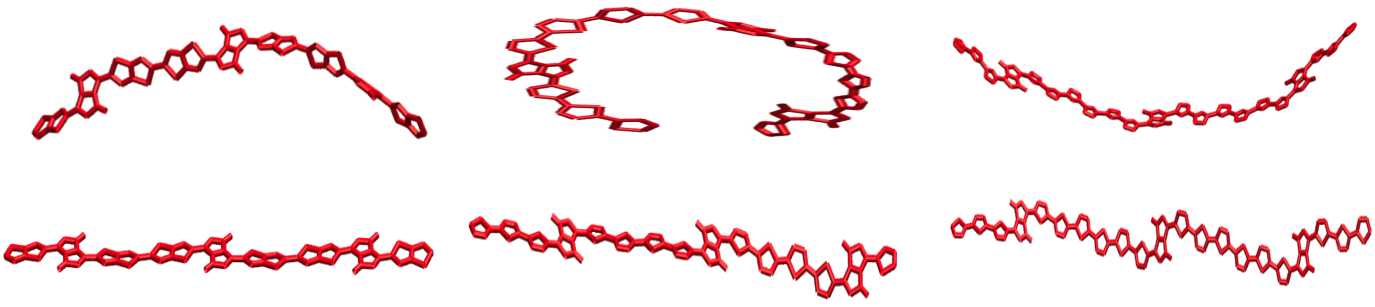

(a) 2TT (b) 4T (c) 6T

Figure 4: Most coiled (in the top panel) and most elongated (in the bottom panel) chains are selected for the three systems showing the variation of flexibility. For the case of 2TT and 6T, individual chains can bend slightly but do not fold, however, folding is visible for the case of 4T.

Radial Distribution Function (RDF)

Radial distribution function (RDF) is calculated for different atom groups of the systems and are compared within and across systems to understand similarities or differences in the systems. Pair distribution function between different atom groups were also used to investigate any preferred direction of chain stacking. Figure.5 shows the RDFs plotted for different atom groups for each system in a separate panel accompanied with cartoons. The strong peak for the DPP belt-belt RDF for the case of 2TT vs DPP belt-S for the case of 6T indicate that the π-stacking in the case of 2TT is formed in a way that the DPP units are aligned whereas the DPP unit alignes with a thiophene unit in the case of 6T forming a step-wise chain stacking. There is a less preferred ordering for the case of 4T as it exhibits the most disordered structure between the three.

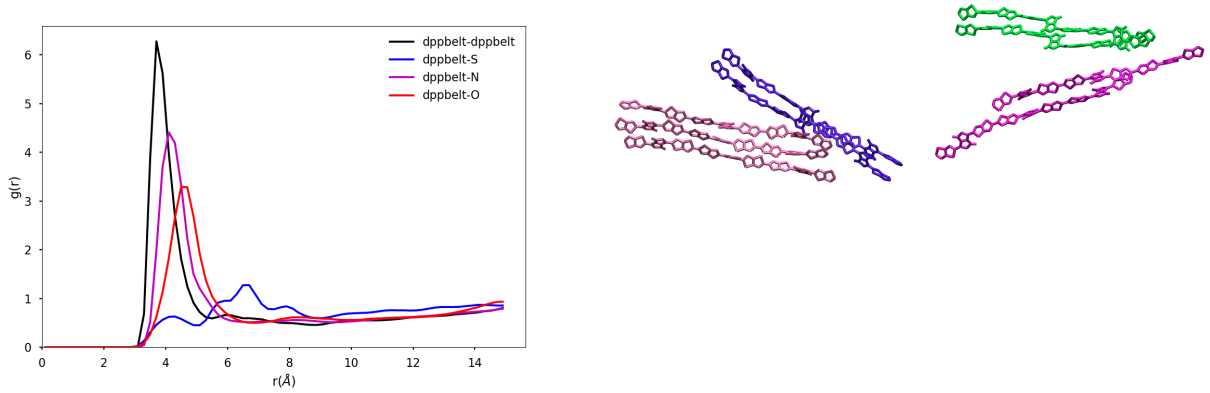

(a) 2TT

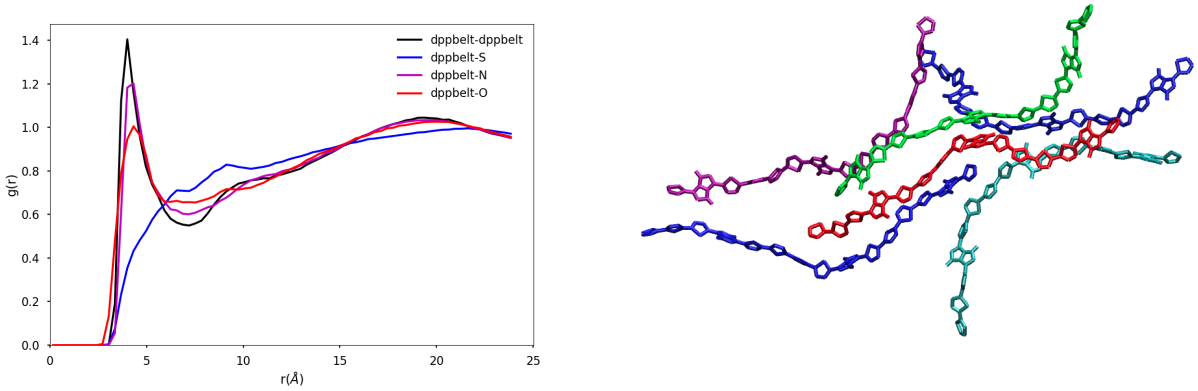

(b) 4T

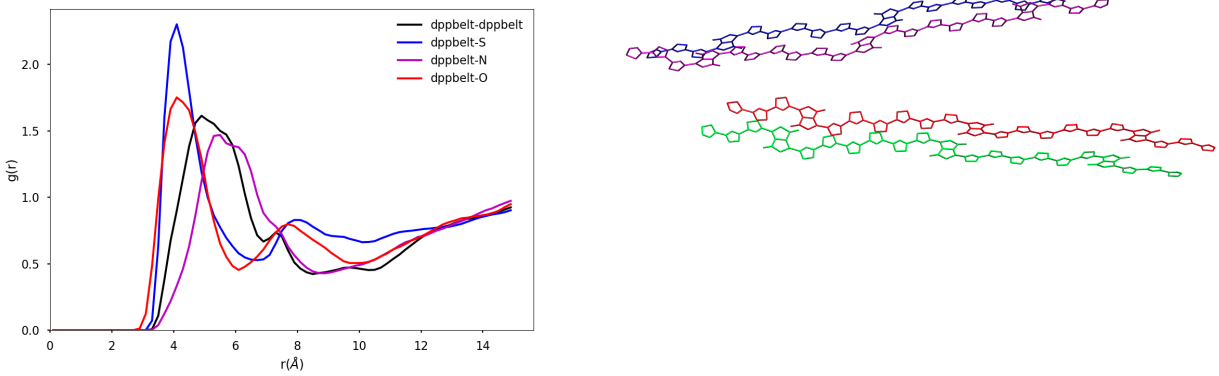

(c) 6T

Figure 5: RDFs plotted for the intra-chain atom groups belonging to the conjugated backbone of the systems to study any preferential direction in the chain stacking. Right panel represents a selection of paired chains.

Figure.6 compares the RDFs plotted for the same atom group for different systems. The higher peak for the system of 2TT in all cases indicates a higher number of stacked chains for

this system. There is a lower amount of ordering evidenced in all panels for 4T in agreement with previous analysis making this systems the least ordered. Studying the positioning of the peaks for N-N and O-O shows that 6T has a higher peak position fir N-N at above 5 $\AA$ and has a lower peak position for O-O at around 3 $\AA$ compared to 2TT and 4T. This is another indication of step-wise stacking in the 6T chains. The RDFs provide a quite comprehensive view of the tendency of DPP polymer to aggregate. Considering the results globally we should differentiate between different characteristics which would be misleading to consider together. First, the tendency of form stable pi-staking interactions decreases in the order 2TT > 6T > 4T. On the other hand, the tendency to form greater aggregates with follow a different order 6T > 2TT > 4T.

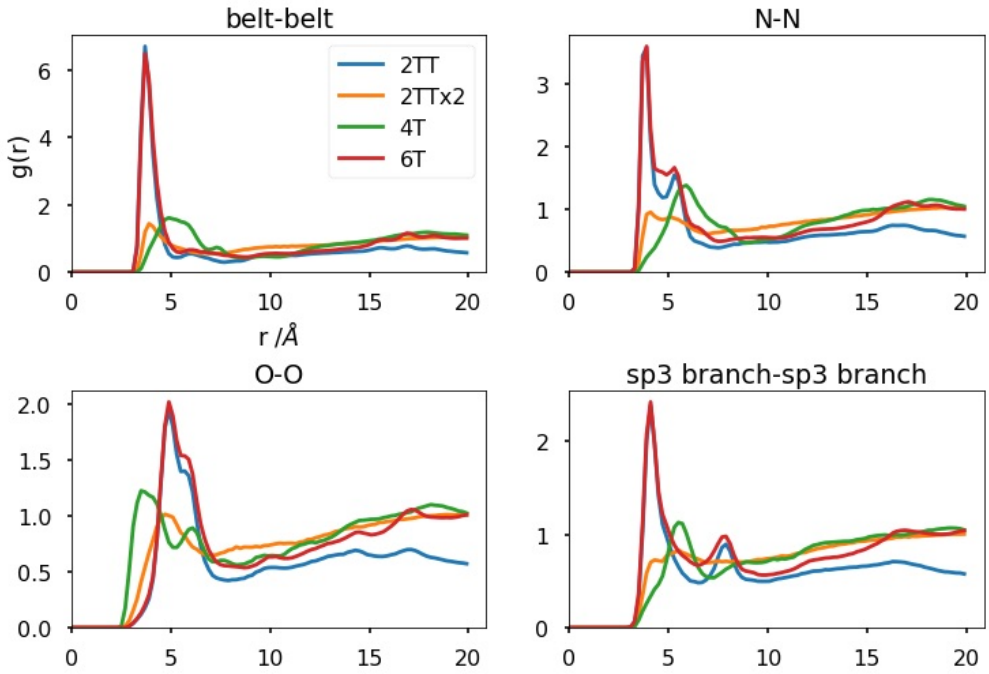

Figure 6: RDFs comparing different atom groups between the systems.

Root Mean Square Displacement

Root mean square displacement (RMSD) per atom type can be used as an indication of which parts are moving more or faster and which atomic groups most influencing the overall displacement of polymer chains. Fig.7 shows RMSD calculated for different atom groups as

well as all atoms. In the case of 4T, which was previously discussed to be the most disordered and flexible system, all atom groups seem to be following the same trend with little to no difference between the overall RMSD and the RMSD of different atom group. For 2TT and 6T, however, it is shown that the higher RMSD for all atoms compared to the atom groups belonging to the backbone is a consequence of a higher RMSD for carbon atoms in the alkyl side chain. This is an indication of higher flexibility of side chains in these two systems. This difference is of a higher order in 6T which is an indication of alkyl chains having more space to move around due to the two extra thiophene rings in the backbone. In the case of 2TT, which is more pronounced for the larger system of 2TTx2, the difference could be a consequence of higher degree of backbone stacking and segregation of backbone and side chains.

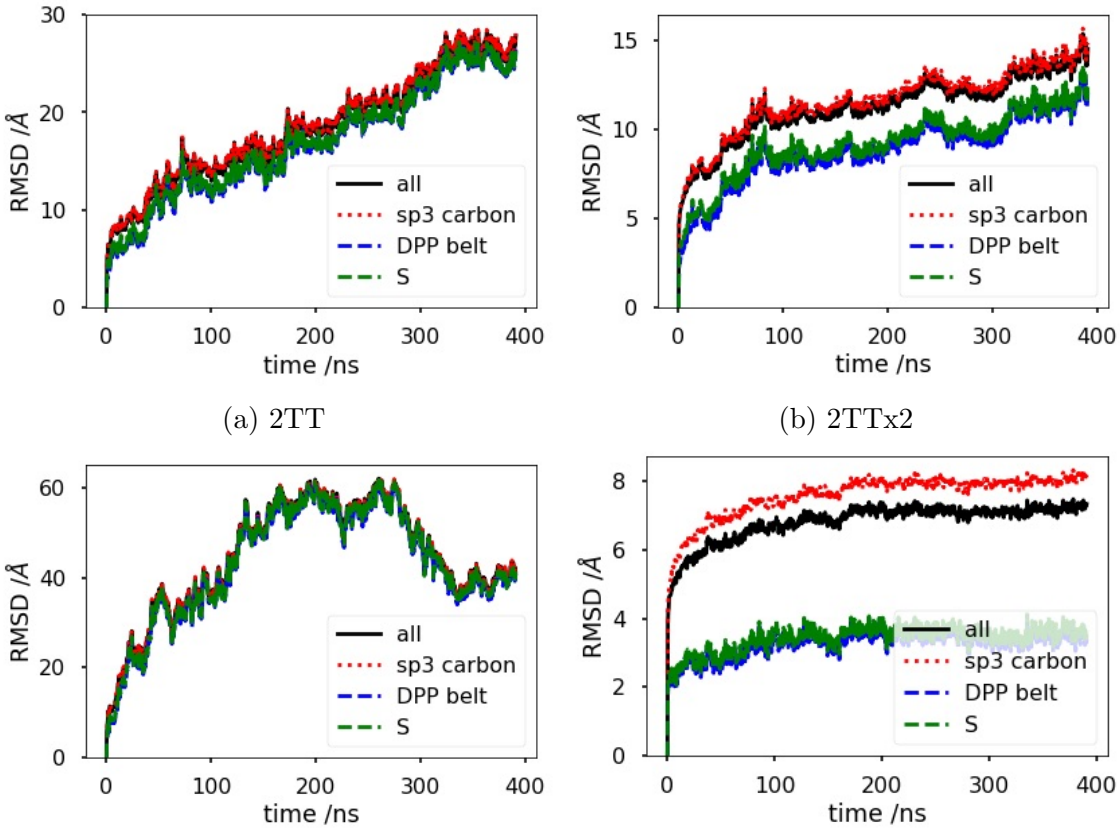

(a) 2TT (b) 2TTx2

(c) 4T (d) 6T

Figure 7: MSD calculations on the three systems showing that there is a greater range of movement associated with the atoms in the side chain for the case of 6T followed by 2TT and 4T.

Conclusion

Atomic MD simulation techniques was employed to study the local structuring and morphological characteristics of three oligorms belonging to the same DPP-base family of SCPs with substituting or adding segments along the backbone unit. All three polymers have reported high charge carrier mobilities realised experimentally. However, it is only with the help of the state of the art simulations that one can see the difference and similarities between them at an atomic scale. Comparing the values calculate for structural properties of the polymer chains such as the radius of gyration (R_g) and end-to-end distances (D_{ee}) showed that all three systems were overall rigid, however, not in the same way. 2TT is the most

homogeneously rigid system followed by 6T while 4T exhibits a wider range of flexibility between individual chains with some almost folded. Strong aggregation at short distances was observed for all three systems and was quantitatively analysed using RDF that showed stacking of up to 6 chains for 2TT and was reduced for 6T and 4T. The existence of peaks in the pair correlation of DPP unit and thiophene rings indicated a preferred step-wise stacking for 6T. The flexibility of different part of a polymeric chains were investigated using the root mean square displacement (RMSD) calculations. It was showed that the side chains are most flexible and free to move around in the case of a more rigid backbone (2TT) proposing a segregation of backbone and side chains, while their movement in 6T is as a result of a bigger spacing in between them for having a longer backbone. In essence, the polymers containing the DPP fragments have a tendency to form aggregates driven by the DPP-DPP interaction, however, this tendency is highly modulated by the polymer composition, which is able to influence the flexibility and the tendency to form stacked aggregates.

Acknowledgements

We are grateful to PRACE for providing computational resources for this work (Project number: 2018184449).

References

(1) Root, S. E.; Savagatrup, S.; Printz, A. D.; Rodriquez, D.; Lipomi, D. J. *Chem. Rev.* **2017**, *117*, 6467–6499.

(2) Gelinck, G.; Heremans, P.; Nomoto, K.; Anthopoulos, T. D. *Adv. Mater.* **2010**, *22*, 3778–3798.

(3) Wu, W.; Liu, Y.; Zhu, D. *Chem. Soc. Rev.* **2010**, *39*, 1489–1502.

(4) Yi, Z.; Wang, S.; Liu, Y. *Adv. Mater.* **2015**, *27*, 3589–3606.

(5) Yoneya, M.; Matsuoka, S.; Tsutsumi, J.; Hasegawa, T. *J. Mater. Chem. C* **2017**, *5*, 9602–9610.

(6) Kawanabe, Y.; Moule, A. J.; Faller, R. *J. Chem. Eng. Data.* **2014**, *59*, 2982–2986.

(7) Sun, T.; Han, J.; Liu, S.; Wang, X.; Wang, Z. Y.; Xie, Z. *Am. Chem. Soc. Nano* **2019**,

(8) Wang, G.-J. N.; Gasperini, A.; Bao, Z. *Adv. Electron. Mater.* **2018**, *4*, 1700429.

(9) Wang, S.; Xu, J.; Wang, W.; Wang, G.-J. N.; Rastak, R.; Molina-Lopez, F.; Chung, J. W.; Niu, S.; Feig, V. R.; Lopez, J. *Nature* **2018**, *555*, 83.

(10) Yun, H.-J.; Lee, G. B.; Chung, D. S.; Kim, Y.-H.; Kwon, S.-K. *Adv. Mater.* **2014**, *26*, 6612–6616.

(11) Facchetti, A. *Chem. Mater.* **2011**, *23*, 733–758.

(12) Ong, B. S.; Wu, Y.; Liu, P.; Gardner, S. *J. Am. Chem. Soc.* **2004**, *126*, 3378–3379.

(13) Do, K.; Ravva, M. K.; Wang, T.; Bredas, J.-L. *Chem. Mater.* **2016**, *29*, 346–354.

(14) Poelking, C.; Cho, E.; Malafeev, A.; Ivanov, V.; Kremer, K.; Risko, C.; Bredas, J.-L.; Andrienko, D. *J. Phys. Chem. C* **2013**, *117*, 1633–1640.

(15) Liu, T.; Troisi, A. *Adv. Funct. Mater.* **2014**, *24*, 925–933.

(16) Alexiadis, O.; Mavrantzas, V. G. *Macromolecules* **2013**, *46*, 2450–2467.

(17) Brocorens, P.; Van Vooren, A.; Chabinyc, M. L.; Toney, M. F.; Shkunov, M.; Heeney, M.; McCulloch, I.; Cornil, J.; Lazzaroni, R. *Adv. Mater.* **2009**, *21*, 1193–1198.

(18) Sirringhaus, H. *Adv. Mater.* **2014**, *26*, 1319–1335.

(19) Heintges, G. H.; Hendriks, K. H.; Colberts, F. J.; Li, M.; Li, J.; Janssen, R. A. *RSC Adv.* **2019**, *9*, 8740–8747.

(20) Selivanova, M.; Chuang, C.-H.; Billet, B.; Malik, A.; Xiang, P.; Landry, E.; Chiu, Y.-C.; Rondeau-Gagné, S. *ACS. Appl. Mater. Inter.* **2019**,

(21) Darling, S. B.; Sternberg, M. *J. Phys. Chem. B* **2009**, *113*, 6215–6218.

(22) Kang, I.; Yun, H.-J.; Chung, D. S.; Kwon, S.-K.; Kim, Y.-H. *J. Am. Chem. Soc.* **2013**, *135*, 14896–14899.

(23) Kline, R. J.; DeLongchamp, D. M.; Fischer, D. A.; Lin, E. K.; Heeney, M.; McCulloch, I.; Toney, M. F. *Appl. Phys. Lett.* **2007**, *90*, 062117.

(24) Jackson, N. E.; Kohlstedt, K. L.; Savoie, B. M.; Olvera de la Cruz, M.; Schatz, G. C.; Chen, L. X.; Ratner, M. A. *J. Am. Chem. Soc.* **2015**, *137*, 6254–6262.

(25) Tamayo, A. B.; Tantiwiwat, M.; Walker, B.; Nguyen, T.-Q. *J. Phys. Chem. C* **2008**, *112*, 15543–15552.

(26) Ponnappa, S. P.; Arumugam, S.; Spratt, H. J.; Manzhos, S.; OMullane, A. P.; Ayoko, G. A.; Sonar, P. *J. Mater. Res.* **2017**, *32*, 810–821.

(27) Yiu, A. T.; Beaujuge, P. M.; Lee, O. P.; Woo, C. H.; Toney, M. F.; Frechet, J. M. *J. Am. Chem. Soc.* **2012**, *134*, 2180–2185.

(28) Lee, J. S.; Son, S. K.; Song, S.; Kim, H.; Lee, D. R.; Kim, K.; Ko, M. J.; Choi, D. H.; Kim, B.; Cho, J. H. *Chem. Mater.* **2012**, *24*, 1316–1323.

(29) Meager, I.; Ashraf, R. S.; Mollinger, S.; Schroeder, B. C.; Bronstein, H.; Beatrup, D.; Vezie, M. S.; Kirchartz, T.; Salleo, A.; Nelson, J. *J. Am. Chem. Soc.* **2013**, *135*, 11537–11540.

(30) Ashraf, R. S.; Meager, I.; Nikolka, M.; Kirkus, M.; Planells, M.; Schroeder, B. C.; Holliday, S.; Hurhangee, M.; Nielsen, C. B.; Sirringhaus, H. *J. Am. Chem. Soc.* **2015**, *137*, 1314–1321.

(31) Tang, M.; Wu, S.; Xing, W.; Shen, H.; Xiang, L.; Liang, Y.; Xu, W.; Zhu, D. *Dyes and Pigments* **2019**, *163*, 707–714.

(32) Zhang, K.; Wucher, P.; Marszalek, T.; Babics, M.; Ringk, A.; Blom, P. W.; Beaujuge, P. M.; Pisula, W. *Chem. Mater.* **2018**, *30*, 5032–5040.

(33) Noriega, R.; Rivnay, J.; Vandewal, K.; Koch, F. P.; Stingelin, N.; Smith, P.; Toney, M. F.; Salleo, A. *Nat. Mater.* **2013**, *12*, 1038.

(34) Nelson, T. L.; Young, T. M.; Liu, J.; Mishra, S. P.; Belot, J. A.; Balliet, C. L.; Javier, A. E.; Kowalewski, T.; McCullough, R. D. *Adv. Mater.* **2010**, *22*, 4617–4621.

(35) Bürgi, L.; Turbiez, M.; Pfeiffer, R.; Bienewald, F.; Kirner, H.-J.; Winnewisser, C. *Adv. Mater.* **2008**, *20*, 2217–2224.

(36) Snyder, C. R.; DeLongchamp, D. M.; Nieuwendaal, R. C.; Herzing, A. A. *Semiconducting Polymers: Controlled Synthesis and Microstructure* **2016**, *21*, 219.

(37) Li, W.; Hendriks, K. H.; Wienk, M. M.; Janssen, R. A. *Acc. Chem. Res.* **2015**, *49*, 78–85.

(38) Zhao, C.; Guo, Y.; Zhang, Y.; Yan, N.; You, S.; Li, W. *J. Mater. Chem. A* **2019**,

(39) Sim, K.; Palai, A. K.; Tarsoly, G.; Na, H.; Pyo, S. *Synth. Met.* **2019**, *250*, 152–160.

(40) Negash, A.; Genene, Z.; Eachambadi, R. T.; Kesters, J.; Van den Brande, N.; DHaen, J.; Penxten, H.; Abdulahi, B. A.; Wang, E.; Vandewal, K. *J. Mater. Chem. C* **2019**, *7*, 3375–3384.

(41) Bijleveld, J. C.; Zoombelt, A. P.; Mathijssen, S. G.; Wienk, M. M.; Turbiez, M.; de Leeuw, D. M.; Janssen, R. A. *J. Am. Chem. Soc.* **2009**, *131*, 16616–16617.

(42) Zhang, S.; Ocheje, M. U.; Huang, L.; Galuska, L.; Cao, Z.; Luo, S.; Cheng, Y.-H.; Ehlenberg, D.; Goodman, R. B.; Zhou, D. *Adv. Electron. Mater.* **2019**, 1800899.

(43) Li, Y.; Singh, S. P.; Sonar, P. *Adv. Mater.* **2010**, *22*, 4862–4866.

(44) Osaka, I.; Takimiya, K. *Polymer* **2015**, *59*, A1–A15.

(45) Baggioli, A.; Casalegno, M.; Raos, G.; Muccioli, L.; Orlandi, S.; Zannoni, C. *Chem. Mater.* **2019**, *31*, 7092–7103.

(46) Caputo, S.; De Nicola, A.; Donati, G.; David, A.; Raos, G.; Milano, G. *J. Electrochem.* **2019**, *166*, B3309–B3315.

(47) Casalegno, M.; Nicolini, T.; Famulari, A.; Raos, G.; Po, R.; Meille, S. V. *Phys. Chem. Chem. Phys.* **2018**, *20*, 28984–28989.

(48) Kotadiya, N. B.; Mondal, A.; Blom, P. W.; Andrienko, D.; Wetzelaer, G.-J. A. *Nature materials* **2019**, *18*, 1182–1186.

(49) Abbaszadeh, D.; Kunz, A.; Kotadiya, N. B.; Mondal, A.; Andrienko, D.; Michels, J. J.; Wetzelaer, G.-J. A.; Blom, P. W. *Chem. Mater.* **2019**, *31*, 6380–6386.

(50) others,, et al. *PNAS* **2018**, *115*, E8341–E8348.

(51) Wolf, C. M.; Kanekal, K. H.; Yimer, Y. Y.; Tyagi, M.; Omar-Diallo, S.; Pakhnyuk, V.; Luscombe, C. K.; Pfaendtner, J.; Pozzo, L. D. *Soft matter* **2019**, *15*, 5067–5083.

(52) Mollinger, S. A.; Krajina, B. A.; Noriega, R.; Salleo, A.; Spakowitz, A. J. *ACS. Macro. Lett.* **2015**, *4*, 708–712.

(53) Henry, M. M.; Jones, M. L.; Oosterhout, S. D.; Braunecker, W. A.; Kemper, T. W.; Larsen, R. E.; Kopidakis, N.; Toney, M. F.; Olson, D. C.; Jankowski, E. *J. Phys. Chem. C* **2017**, *121*, 26528–26538.

(54) others,, et al. *J. Am. Chem. Soc.* **2011**, *133*, 3272–3275.

(55) Hoang, M. H.; Nguyen, D. N.; Ngo, T. T.; Um, H. A.; Cho, M. J.; Choi, D. H. *Polymer* **2016**, *83*, 77–84.

(56) Hoang, Q. V.; Song, C. E.; Kang, I.-N.; Moon, S.-J.; Lee, S. K.; Lee, J.-C.; Shin, W. S. *RSC advances* **2016**, *6*, 28658–28665.

(57) others,, et al. *ACS applied materials & interfaces* **2016**, *8*, 12940–12950.

(58) Ha, J. S.; Kim, K. H.; Choi, D. H. *J. Am. Chem. Soc.* **2011**, *133*, 10364–10367.

(59) Allen, M. P.; Tildesley, D. J. *Computer simulation in chemical physics*; Springer Science & Business Media, 2012; Vol. 397.

(60) Jorgensen, W. L.; Maxwell, D. S.; Tirado-Rives, J. *J. Am. Chem. Soc.* **1996**, *118*, 11225–11236.

(61) Breneman, C. M.; Wiberg, K. B. *J. Comput. Chem.* **1990**, *11*, 361–373.

(62) Frisch, M. J.; Head-Gordon, M.; Pople, J. A. *Chem. Phys. Lett.* **1990**, *166*, 275–280.

(63) Frisch, M. J.; Head-Gordon, M.; Pople, J. A. *Chem. Phys. Lett.* **1990**, *166*, 281–289.

(64) Plimpton, S. *J. Comput. Phys.* **1995**, *117*, 1–19.

(65) McCulloch, I.; Heeney, M.; Bailey, C.; Genevicius, K.; MacDonald, I.; Shkunov, M.; Sparrowe, D.; Tierney, S.; Wagner, R.; Zhang, W. *Nat. Mater.* **2006**, *5*, 328.